The final publication is available at Springer via http://dx.doi.org/10.1007/s10933-015-9833-7

Holocene sea level and environmental change on the west coast of South Africa: evidence from plant biomarkers, stable isotopes and pollen

Andrew S Carr*[1], Arnoud Boom[1], Brian M Chase[2, 3], Michael E Meadows[4], Hannah L Grimes[1]

1: Department of Geography, University of Leicester, University Road, Leicester, LE1 7RH, UK: asc18@le.ac.uk, ab269@le.ac.uk

2: Institut des Sciences de l'Evolution de Montpellier, UMR 5554, Centre National de Recherche Scientifique/Université Montpellier 2, Bat.22, CC061, Place Eugène Bataillon, 34095 Montpellier, cedex5, France brian.chase@univ-montp2.fr

3: Department of Archaeology, History, Culture and Religion, University of Bergen, Postbox 7805, 5020, Bergen, Norway

4: Department of Environmental and Geographical Science, University of Cape Town, Private Bag X3, Rondebosch 7701, South Africa

*Corresponding author. Email: asc18@le.ac.uk, Tel: +44 (0) 116 2523851

Keywords: Western Cape, Sea level, Stable isotopes, Leaf wax, py-GC/MS, Thiophene ratio

The final publication is available at Springer via http://dx.doi.org/10.1007/s10933-015-9833-7

Abstract

We present an 8,000-year biomarker and stable carbon isotope record from the Verlorenvlei Estuary, South Africa. We assessed how leaf wax lipids, insoluble macromolecular organic matter, bulk C/N data and compound-specific stable carbon isotopes were linked to the site's palynological record and to evidence for regional sea level and environmental change. Down-core trends in bulk $\delta^{13}C$ are closely coupled to trends in pollen types from saline-tolerant taxa. These trends are mirrored by variations in the incorporation of reduced sulphur into macromolecular organic matter. This process, quantified with the thiophene ratio, is closely associated with periods of higher sea level 8,000-4,300 cal yr BP. We propose the thiophene ratio is a proxy for relative marine influence within (peri) estuarine sediments. All measured variables indicate differences between early-middle Holocene (8,000-4,300 cal BP) and late Holocene conditions at Verlorenvlei. The former period was more saline and preserves more labile macromolecular organic matter. Marine influence declined after 4,300 cal yr BP, and although the abundance of short-chain-length *n*-alkanes suggests continued presence of wetland flora until 2,500 cal yr BP, organic matter preservation became poorer and a drying trend was inferred, most notably for the interval 2,500-900 cal BP. Increasing freshwater inundation is apparent during the last 700 cal years, consistent with several records from this region. Leaf wax *n*-alkane distributions are largely uncorrelated with bulk organic matter variables, with the exception of the abundance of C_{31} and C_{33} *n*-alkanes, which are negatively correlated with $\delta^{13}C_{TOC}$. Furthermore, C_{31}-C_{33} *n*-alkane $\delta^{13}C$ values are uncorrelated with C_{23}-C_{29} $\delta^{13}C$ and $\delta^{13}C_{TOC}$. They are also higher than our newly measured terrestrial (C_3) vegetation C_{29} and C_{31} end-member values of -35 ± 2 and -34 ± 1‰, respectively. These patterns are best explained by a dominant contribution of local riparian vegetation to the C_{23}-C_{29} *n*-alkanes, but time-varying contributions of non-local leaf waxes to the C_{31}-C_{33} signals. This renders inferences concerning regional environmental change from long-chain leaf waxes potentially challenging in this setting.

The final publication is available at Springer via http://dx.doi.org/10.1007/s10933-015-9833-7

Introduction

The coastal plains of the South African west coast, known locally as the Sandveld (Fig. 1), represent a region of considerable palaeoenvironmental interest (Chase and Meadows 2007). The region is characterized by the interaction of large-scale atmospheric circulation systems over southwest South Africa, specifically the mid-latitude westerly systems and the South Atlantic Anticyclone (Stager et al. 2012), and possesses an important archaeological record (Parkington et al. 1988; Parkington 2012). The coastal lowlands also form part of the mega-diverse Cape Floristic Region, with the Sandveld representative of the Lowland Fynbos eco-region. Palaeoecological records from this region are scarce, reflecting the rare accumulation of organic-rich sediments under largely semi-arid conditions (Chase and Meadows 2007).

An exception is the Verlorenvlei River system (Fig. 1), which has yielded several Holocene sediment records, enabling reconstructions of vegetation history (Baxter, 1997; Meadows et al. 1994, 1996; Meadows and Baxter 2001), lake salinity (Stager et al. 2012), sea-level change (Baxter and Meadows 1999), shifting sediment provenance (Meadows and Asmal 1996) and post-colonial impacts (Baxter and Meadows 1994). Although providing some insights into the region's environmental dynamics, these records are generally short and/or contain depositional hiatuses. Additionally, the interpretation of pollen records from this region, and semi-arid areas in general, is challenging. Pollen spectra are frequently dominated by over-represented pollen from grasses and/or the immediate wetland environment (Horowitz 1992). Combined with the low taxonomic resolution of many pollen morphotypes in this region, assessing regional palaeoenvironmental signals has proved difficult. The most complete Holocene pollen record reported for the Sandveld is the Klaarfontein deposit, which lies on the inland margin of the Verlorenvlei River, approximately 1.9 m above modern sea level (Meadows and Baxter 2001; henceforth, core KFN1996 [Fig. 1]). This record spans the last *ca*. 8,000 cal years and its associated pollen spectra were previously inferred to have been strongly influenced by saline-tolerant riparian taxa, indicative of varying marine influence within the Verlorenvlei system. Following a reduction in marine influence during the late Holocene

The final publication is available at Springer via http://dx.doi.org/10.1007/s10933-015-9833-7

and a commensurate reduction in the abundance of these riparian pollen types, more subtle adjustments in wetland and terrestrial vegetation communities were inferred (Meadows et al. 1996; Baxter and Meadows 1999; Meadows and Baxter 2001), although the timing and precise significance of these changes were difficult to assess.

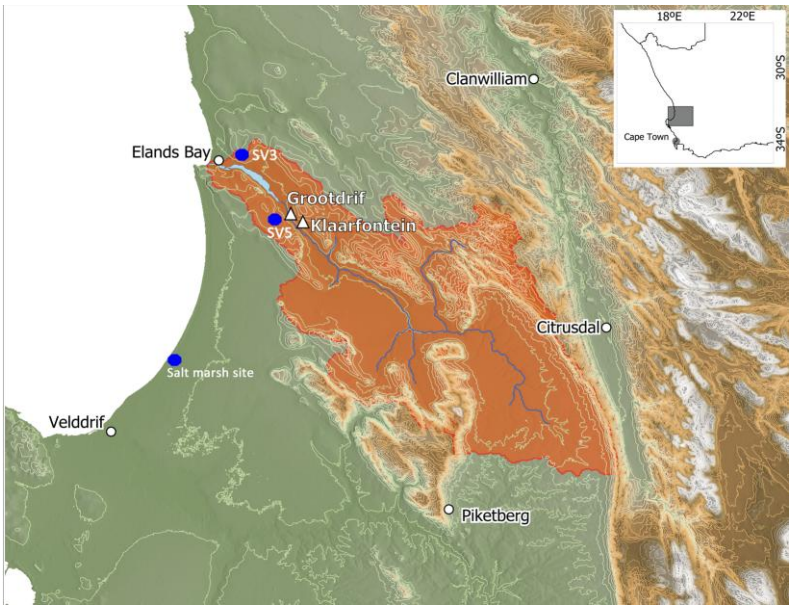

Fig. 1 Map of the study area including the location of the Klaarfontein site, the approximate catchment area of the Verlorenvlei Estuary and the locations of the modern soil samples

In this study, we revisit Klaarfontein and present a new suite of climate and environmental proxy data, along with a revised chronology for the site. We sought to provide more detailed insights into the site's (and the Sandveld region's) environmental history, and through the application of multiple stable isotope and plant biomarker proxies, to explore the use and interpretation of these organic geochemical proxies in semi-arid regions. The study goals were to: 1) explore how multiple organic geochemical variables can be used to provide insights into local and regional ecological changes in this semi-arid setting, 2) assess how biomarker and compound-specific stable isotope values are linked to the site's palynological record, 3) improve temporal constraints for this site and the wider Verlorenvlei system and, 4) expand our understanding of local and regional environmental

history. As one of the more complete Holocene sediment archives for the west coast, Klaarfontein represents an important, but potentially under-exploited Holocene environmental archive, and may serve as a counterpoint for palaeoecological records in the adjacent Western Cape mountains (Scott and Woodborne 2007).

A key goal was to assess how organic geochemical variables relate to the site's palynological record and whether application of several geochemical proxies, related to different organic matter (OM) fractions and potentially derived from different sources (i.e. locally-derived macromolecular organic matter verses more widely dispersed leaf wax lipids), can provide insights into the site history and the regional palaeoenvironment. To this end, we analysed total organic carbon (TOC), $\delta^{13}C_{TOC}$, total nitrogen (TN), and TOC/TN ratios to consider the basic OM character, provenance (Lamb et al. 2004) and isotopic signature (Wang et al. 2003), along with solvent-extractable leaf wax lipids from terrestrial higher plants, and the solvent-insoluble macromolecular organic residue. Among the extractable lipids, the relative abundance of C_{21}-C_{33} leaf wax *n*-alkanes is known to vary with plant type and across environmental gradients (Rommerskirchen et al. 2003; Carr et al. 2014). Such leaf waxes can be widely dispersed, but in lake and wetland settings shorter-chain-length *n*-alkanes (C_{23}-C_{25}) tend to be more abundant in aquatic and riparian plants. This enables assessment of the contribution of aquatic/riparian plants to sediment organic matter (Ficken et al. 2000; Aichner et al. 2010; Gao et al. 2011). In combination with compound-specific stable carbon isotope data, and assuming that particular leaf waxes are derived from different plant sources, such analyses have been used to distinguish between local and regional-scale environmental signals. Pyrolysis-gas chromatography/mass spectrometry (py-GC/MS) can be used to characterise solvent-insoluble macromolecular sediment organic matter. Py-GC/MS fragments macromolecules (e.g. lignin) into GC-amenable pyrolysis products, from which the original macromolecular composition is inferred (de Leeuw et al. 2006). This provides insights into organic matter preservation and post-depositional alteration, organic matter sources (e.g. algal verses higher plant biomass contributions) and palaeoenvironmental conditions (Kaal et al. 2014). To assist in the interpretations of these variables,

The final publication is available at Springer via http://dx.doi.org/10.1007/s10933-015-9833-7

we also present new data pertaining to the biomarker and stable isotope fingerprints of modern plant-derived organic matter from the area, building on several recent studies (Boom et al. 2014; Carr et al. 2014).

Materials and methods

Site description

The Verlorenvlei system is a narrow (13 x 1.5 km) and shallow (maximum depth 5 m) coastal water body comprised of a river and semi-estuarine coastal lake surrounded by reed swamp (Sinclair et al. 1986; Meadows and Asmal 1996; Stager et al. 2012). The lake is connected to the sea by a short channel, but because of a sand bar at the estuary mouth, apart from rare storm events and spring tides, there is limited input of seawater from the Atlantic Ocean (Sinclair et al. 1985; Miller et al. 1995). Heavy winter rain in the catchment can mean that the estuary channel overtops the bar and flows into the sea. Today, water salinity varies from ~12 parts per thousand near the estuary mouth to <1 part per thousand near Rederlinghuys (Sinclair et al. 1986; Fig. 1). Verlorenvlei is generally considered to be oligotrophic, although the nutrient status and phytoplankton activity vary significantly, reflecting variability in freshwater input and evaporation under a semi-arid and strongly seasonal climate (Sinclair et al. 1986; Stager et al. 2012).

Klaarfontein itself lies on the northern margin of the Verlorenvlei River, approximately 18 km from the Atlantic Ocean (Fig. 1) and 3 km from the Grootdrift site (Baxter and Meadows 1999). It comprises a lobe-shaped marshy alluvial deposit ~2 m above Verlorenvlei, which is covered in *Typha* sp., *Juncus* sp. and various Cyperaceae species. *Phragmites australis* and *Myriophyllum spicatum* fringe the transition to open water. The wider environment comprises the Sandveld coastal plain. To the south, low sandstone hills lie adjacent to the estuary and host sandstone Fynbos vegetation. Vegetation within the catchment is largely associated with sandy substrates and consists of a mixture of woody lowland Fynbos shrubs, restioid Fynbos and karroid communities (Meadows et al. 1994; Meadows and Baxter 2001; Fig. S1). In general, the Verlorenvlei system region lies close to the

The final publication is available at Springer via http://dx.doi.org/10.1007/s10933-015-9833-7

ecotone between the lowland Fynbos and arid-adapted karroid shrublands further north. The climate today is semi-arid, receives the majority of its rainfall (~300 mm a^{-1}) during the winter months and shows significant inter-annual variability.

Sampling, chronology and analyses

In 2010 a 2.3-m vibracore (KFN2010) was obtained from the same location where Meadows and Baxter (2001) retrieved their core. The sealed core was opened and sub-sampled at the University of Cape Town. Samples were shipped to the UK, freeze-dried and homogenised. Additional samples were obtained from modern soils within Sandveld and Sand Fynbos vegetation around Verlorenvlei, to provide contemporary stable isotope and plant biomarker data to compare against the KFN2010 sediments (Fig. 1). These relate to terrestrial soils adjacent to Verlorenvlei, specifically sites SV3 and SV5 described in Carr et al. (2013, 2014), along with samples from a modern salt marsh, 24 km north of Velddrif, south of Verlorenvlei (Fig. 1 and Electronic Supplementary Material [ESM] Fig. 1). This site, now isolated from the sea, is presently dominated by halophytic vegetation, including *Sarcocornia pillansii* (Chenopodiaceae), *Frankenia pulverulenta* (Frankeniaceae) and *Cynodon dactylon* (Poaceae) in subordinate amounts.

Eight bulk sediment samples from KFN2010 were used to construct a radiocarbon chronology. AMS analyses were carried out at the University of Waikato radiocarbon dating laboratory and the ^{14}CHRONO Centre at Queen's University, Belfast (ESM Table 1). Measurements were carried out on the insoluble residue remaining after hot HCl treatment and hot NaOH washes. The final ages are based on percent modern carbon, the Libby half-life (5,568 yr) and isotopic fractionation correction. There is potential for marine contributions to the organic matter at this site (Baxter and Meadows, 1999), but given the dominantly terrestrial character of extracted biomarkers and an absence of concrete evidence for the proportion of marine organic matter contribution, radiocarbon age calibrations for KFN2010 used only the atmospheric curve data (Hogg et al. 2013). Calibration to calendar years was carried out with the Southern Hemisphere atmospheric curve

The final publication is available at Springer via http://dx.doi.org/10.1007/s10933-015-9833-7

SHCal13 (Hogg et al. 2013) using CALIB 7.0 (Stuiver and Reimer 1993). The 2-sigma calibrated age ranges are presented in ESM Table 1. An age-depth model (ESM Fig. 2) was obtained using the Bacon 2.2 software (Blaauw and Christen 2011). To provide summary variables for comparison with the various geochemical proxies and to re-assess local/regional pollen contributions, the original pollen counts from KFN1996 (Meadows and Baxter 2001) were re-analysed with detrended correspondence analysis (DCA) using the PAST software (Hammer et al. 2001). The published radiocarbon ages for KFN1996 were calibrated and an age-depth model developed in the same manner as for KFN2010 (ESM Fig. 3 and ESM Table 1).

Bulk organic geochemistry

Bulk measurements of total organic carbon (TOC), total nitrogen (TN) and $\delta^{13}C_{TOC}$ were made using a SerCon ANCA GSL elemental analyser interfaced to a Hydra 20-20 continuous flow isotope ratio mass spectrometer. Analyses were carried out in triplicate. For TOC and $\delta^{13}C_{TOC}$, the samples were pre-treated with dilute HCl, rinsed in deionised water and freeze dried. TN was determined without acid pre-treatment.

Lipid biomarker and compound-specific $\delta^{13}C$ analyses

Leaf wax lipids (*n*-alkanes) were extracted from ~5 g of powdered sediment using soxhlet extraction (24 hours: hexane, DCM and methanol; ratio 1:2:2). The extracts were rotary evaporated and the apolar fraction was isolated via Al_2O_3 column chromatography using a hexane/DCM mixture (9:1). Gas chromatography was carried out on a Perkin Elmer Clarus 500 GC/MS equipped with a CP-Sil 5CB (30 m x 0.25 mm) column. The GC oven programme involved an initial temperature of 60°C, ramping to 120°C at 20°C min^{-1}, ramping to 325°C at 4°C min^{-1} and a hold at 325°C for 15 minutes. Compounds were identified from their mass spectra and retention times. Linearity between peak area and concentration was checked for all (C_7-C_{40}) *n*-alkanes in the range 0-500 µg mg^{-1}.

The final publication is available at Springer via http://dx.doi.org/10.1007/s10933-015-9833-7

Several indices were used to characterise the leaf wax *n*-alkane distributions. The Carbon Preference Index (CPI), which is a measure of odd over even chain length preference and is used as a measure of *n*-alkane origins, was calculated following Bray and Evans (1961):

$$CPI_{23\text{-}33} = \frac{1}{2}\left(\frac{C23+C25+C27+C29+C31+C33}{C22+C24+C26+C28+C30+C32}\right) + \left(\frac{C23+C25+C27+C29+C31+C33}{C24+C26+C28+C30+C32+C34}\right) \quad (1)$$

Where C_x is the concentration of the *n*-alkane with x carbon atoms.

The average chain length (ACL), which is equivalent to the weighted mean of all odd chain length *n*-alkanes, was calculated following Poynter et al. (1989).

$$ACL_{21\text{-}33} = \frac{21*C21+ 23*C23+25*C25+27*C27+29*C29+31*C31+33*C33}{C21+C23+C25+C27+C29+C31+C33} \quad (2)$$

Where C_x is the concentration of the *n*-alkane with x carbon atoms.

The ratio of short to long chain length *n*-alkanes (the P_{aq} index) was calculated following Ficken et al. (2000):

$$P_{aq} = \frac{(C23+C25)}{(C23+C25+C29+C31)} \quad (3)$$

Various studies have also found the ratio between the C_{29} and C_{31} *n*-alkanes (Norm31) to be an environmentally sensitive parameter. This is calculated as:

$$Norm31 = C_{31}/(C_{31}+C_{29}) \quad (4)$$

where C_x is the concentration of the *n*-alkane (C) with x carbon atoms.

Compound-specific $\delta^{13}C$ analyses of the C_{23}-C_{33} *n*-alkanes from KFN2010 and the modern soils were performed using gas chromatography-isotope ratio monitoring mass spectrometry (irm-GC/MS). An Agilent 6890N gas chromatograph equipped with a platinum-copper wire combustion reactor was interfaced to a SerCon GC-CP and connected to the Hyrda 20-20 MS. Samples were spiked with two laboratory standards (C_{19} FAME and α-cholestane) and were monitored with

The final publication is available at Springer via http://dx.doi.org/10.1007/s10933-015-9833-7

calibrated CO_2 injections at the beginning and end of each GC run. Measurements were carried out in triplicate and the resulting precision was better than 0.5‰ in all replicate samples (Table 1).

Insoluble organic matter

The insoluble organic matter was analysed using py-GC/MS. This fragments complex macromolecular organic matter in an inert (helium) atmosphere to produce lower molecular weight products amenable to GC/MS analysis. Analysis of the resulting products can be used to reconstruct their likely macromolecular progenitors, providing a semi-quantitative assay of organic matter composition and structure (Saiz-Jimenez and de Leeuw 1987). The residues remaining following the soxhlet extraction were pyrolysed at 610°C using a CDS 1000 pyroprobe, interfaced with a Perkin Elmer Clarus 500 GC/MS system (Carr et al. 2013). The compounds within the resulting pyrograms were identified based on their mass spectra and retention times. Peak integrations on the total ion current (TIC) were performed using Turbo-Mass 5.2.0 software. The signal for each compound was determined as a percentage of the total signal from all integrated compounds (Vancampenhout et al. 2008).

Results

Core stratigraphy

The stratigraphy and chronology of KFN2010 are comparable to those for KFN1996 (Baxter 1997; Meadows and Baxter 2001). Notably, the oldest radiocarbon age in KFN2010 (6,621 ± 40 ^{14}C yr BP) is very similar to the basal age in KFN1996 (6,870 ± 90 ^{14}C yr BP (Pta-6148)) and in both instances these lie immediately above a distinct facies change to grey-coloured, medium-coarse-grained sands. Extrapolation from the age-depth model for KFN2010 suggests that these sands date to *ca.* 8,900 cal yr BP. Much of the KFN2010 core, between 2.00 to 0.6 m, is comprised of dark brown to black silts and clays. A distinct layer of mottled black silt-clay at 1.00-1.20 m in KFN2010 is similar in age (4,400-4,300 cal yr BP) to a dark grey clay layer identified at about 2.00 m in KFN1996 (4,000-3,700 cal yr

The final publication is available at Springer via http://dx.doi.org/10.1007/s10933-015-9833-7

BP; 3,640 ^{14}C yr BP; Pta6145). In both cores this marks a clear transition to slower deposition and a more lithologically variable late Holocene. The age-depth model for KFN2010 implies slower deposition 1.00-0.7 m (4,350-1,770 cal yr BP; ESM Table 1; ESM Figs. 2,3). Based on fewer ages Meadows and Baxter (2001) drew a similar conclusion for KFN1996 and suggested there may even be a late Holocene depositional hiatus. Visual inspection of KFN2010, however, does not reveal evidence for a hiatus, but this, or incomplete retrieval of late Holocene sediments, cannot be ruled out at present. Overall, the age models and sedimentology of KFN2010 and KFN1996 compare favourably. The effects of a reduction in sedimentation rate and/or increased sediment compaction during the late Holocene mean that relatively few samples in KFN2010 represent the period 4,000-2,000 cal yr BP, and some caution is needed to interpret this period.

Bulk organic matter

Total organic carbon (TOC) within KFN2010 varies between 0.2 and 6 % (Fig. 2). There are no strong down-core trends in this variable, although TOC is generally higher in the interval 9,000-5,000 cal yr BP, and phases of higher TOC are seen at 7,500, 6,000-4,000 and 580 cal yr BP, along with a pronounced minimum *ca*. 1,200-900 cal yr BP. The early to middle Holocene (9,000-4,500 cal yr BP) is characterised by relatively higher $\delta^{13}C_{TOC}$ (range -24.0 ‰ to -21.7 ‰) and lower TOC/TN (minima: 6,900-6,300 cal yr BP). After *ca*. 6,000 cal yr BP, TOC/TN rises, peaking around 4,000 cal yr BP and remaining high until *ca*. 1,500 cal yr BP. From 5,400 cal yr BP, $\delta^{13}C_{TOC}$ falls, stabilising at -25 ‰ from *ca.* 3,000 to 1,200 cal BP, with a brief minimum at 1,000 cal yr BP. TOC/TN remains relatively high (~20) throughout this period until 1,500 cal yr BP, before dropping towards the top of the core. Modern terrestrial soils surrounding Verlorenvlei (Fig. 1) are characterised by TOCs of 0.4-0.6%, an average TOC/TN ratio of 11 ± 2 and $\delta^{13}C_{TOC}$ typical of soil organic matter in C_3 ecosystems (-25 ± 1 ‰).

The final publication is available at Springer via http://dx.doi.org/10.1007/s10933-015-9833-7

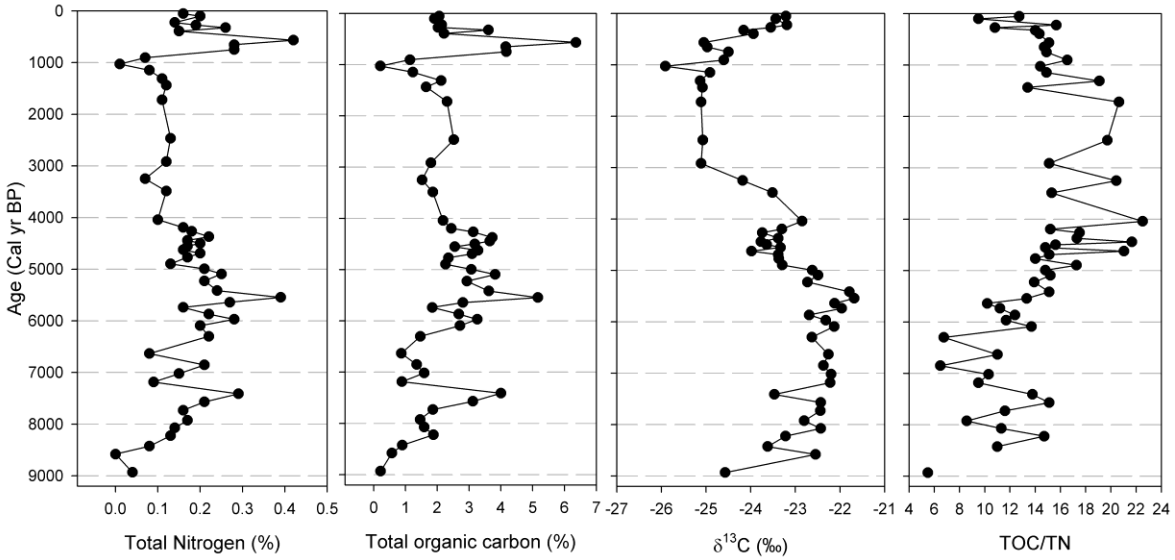

Fig. 2 Down-core trends in total organic carbon, nitrogen and $\delta^{13}C_{TOC}$ for KFN2010, obtained via elemental analysis

Leaf wax *n*-alkanes

All samples contain *n*-alkanes in the range C_{21} to C_{33}, with their total concentration ranging from 0.3 to 7.0 µg g^{-1} dry weight. For *n*-alkanes C_{23}-C_{33}, odd over even chain length preference is clearly apparent ($CPI_{23\text{-}33}$ = 4 to 16, where 1 indicates no odd/even preference), which is indicative of a dominantly higher-plant leaf wax origin. Down core, the C_{23}-C_{33} *n*-alkanes show marked changes in distribution and concentration (Fig. 3 and ESM Fig. 4) and there is particular variability in the ratio of short (C_{23}-C_{25}) to long (C_{29}-C_{31}) chain length *n*-alkanes, as measured by the P_{aq} index (Fig. 3).

From 8,000 cal yr BP, the P_{aq} index increases steadily, indicating an increasing contribution of shorter chain length (C_{23}-C_{25}) *n*-alkanes. This trend continues until *ca*. 2,500 cal BP, whereupon there is a shift towards a greater proportion of longer-chain-length *n*-alkanes. This trend of increasing $ACL_{21\text{-}33}$, decreasing P_{aq} and increasing CPI culminates at *ca.* 900 cal yr BP, where chain lengths < C_{29} almost disappear. Following this, there is an abrupt reversal and the last 900 years are more typical

The final publication is available at Springer via http://dx.doi.org/10.1007/s10933-015-9833-7

of the rest of the core, displaying a wider spread of *n*-alkane chain lengths (higher P_{aq}), lower ACL_{21-33} and lower CPIs. Overall, the variation in ACL_{21-33} is driven largely by the contribution of shorter (C_{23}-C_{27}) *n*-alkanes. Variability in the relative abundance of the longest-chain-length alkanes (C_{29}-C_{33}, also represented by the Norm31 parameter) is more muted and the Norm31 values are comparable to modern plant values throughout (Fig. 3). Chain-length distributions tend to be longest during the last 3,000 years and in the interval 9,000-7,500 cal yr BP. The only statistically significant correlations between the *n*-alkane distributions and the bulk organic matter variables are associated with the C_{29}-C_{33} chain lengths, and are seen in the negative correlations between Norm31 and ACl_{27-33} (note the longer ACL range here than described above) and $\delta^{13}C_{TOC}$ (Spearman's Rho of -0.54 and $p< 0.01$ for both lipid variables).

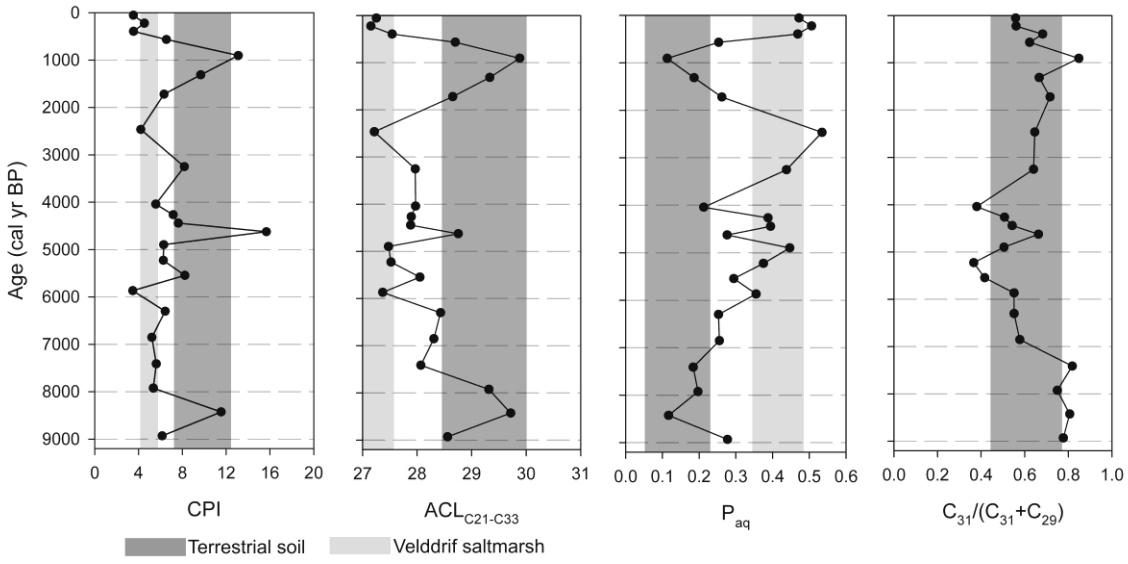

Fig. 3 Down-core trends in leaf wax *n*-alkane distribution descriptive parameters. Shadings indicate one standard deviation ranges for the Velddrif salt marsh and for terrestrial soils in the Sandveld, the latter using all Lowland Fynbos eco-region data reported in Carr et al. (2014). For the Norm31 - $C_{31}/(C_{31}+C_{29})$ the salt marsh and terrestrial averages overlap almost exactly

The final publication is available at Springer via http://dx.doi.org/10.1007/s10933-015-9833-7

290 The ranges in *n*-alkane distributions from modern soils around Verlorenvlei, as previously
291 reported in Carr et al. (2014), are shown as grey boxes in Fig. 3. They are dominated by the C_{31} and
292 C_{29} homologues, with the C_{31} the most abundant (Norm31 averages 0.6 ± 0.2, which is identical to
293 most KFN2010 values). The P_{aq} for terrestrial soil extracts SV3 and SV5 is 0.2 ± 0.2, but may be as
294 high as 0.32, implying some caution is required when interpreting this variable as an indicator of
295 purely aquatic vegetation. In the Velddrif salt marsh the *n*-alkane distribution is wider than the soils
296 and the odd/even chain length preference is less prominent (ESM Fig. 4). The CPI (average 5 ± 1) is
297 more similar to the KFN2010 core samples (average 7 ± 3) than to the terrestrial soils (average 10 ±
298 2), and although C_{31} is the most abundant *n*-alkane, the $C_{23\text{-}27}$ are proportionally higher than the
299 terrestrial soils, with the P_{aq} (0.42 ± 0.7) comparable to parts of KFN2010 (Fig. 3). As in KFN2010, the
300 Norm31 (0.66 ± 0.02) is also similar to the modern soils.

301 **Compound-specific $\delta^{13}C$**

302 The terrestrial soil samples (n=5) $\delta^{13}C_{C29}$ and $\delta^{13}C_{C31}$ average -35 ± 2 ‰ and -34 ± 1 ‰, respectively
303 (Table 1). These data provide new C_3 end-member data for the Sandveld and southernmost South
304 Africa more generally. For KFN2010, *n*-alkane data were obtained for 17 samples (Fig. 4 and Table 1).
305 In KFN2010, $\delta^{13}C_{C25}$, $\delta^{13}C_{C27}$ and $\delta^{13}C_{C29}$ all track $\delta^{13}C_{TOC}$. Correlation coefficients between $\delta^{13}C_{TOC}$ and
306 $\delta^{13}C_{C25}$, $\delta^{13}C_{C27}$ and $\delta^{13}C_{C29}$ are 0.69, 0.86, and 0.80, respectively ($p < 0.001$). In contrast, $\delta^{13}C_{C31}$ and
307 $\delta^{13}C_{C33}$ show no statistically significant correlation with either $\delta^{13}C_{TOC}$ (r=-0.03 and 0.23, p=0.9 and
308 0.4) or the C_{25}-C_{29} homologues (e.g. $\delta^{13}C_{C29}$ and $\delta^{13}C_{C31}$: r=0.2, p=0.5). They exhibit far less down-core
309 variation ($\delta^{13}C_{C31}$ and $\delta^{13}C_{C33}$ averaging -29 ± 2 ‰ and -27 ± 2 ‰, respectively) and, like all of the leaf
310 wax *n*-alkanes extracted from KFN2010, their absolute values are in most cases higher than the
311 terrestrial (C_3 vegetation) Sandveld soils (Table 1). A possible exception is $\delta^{13}C_{C31,}$ which approaches
312 the likely C_3 end-member data from the local soils if a ~2 ‰ correction for the Suess effect is applied
313 (Garcin et al. 2014).

314

The final publication is available at Springer via http://dx.doi.org/10.1007/s10933-015-9833-7

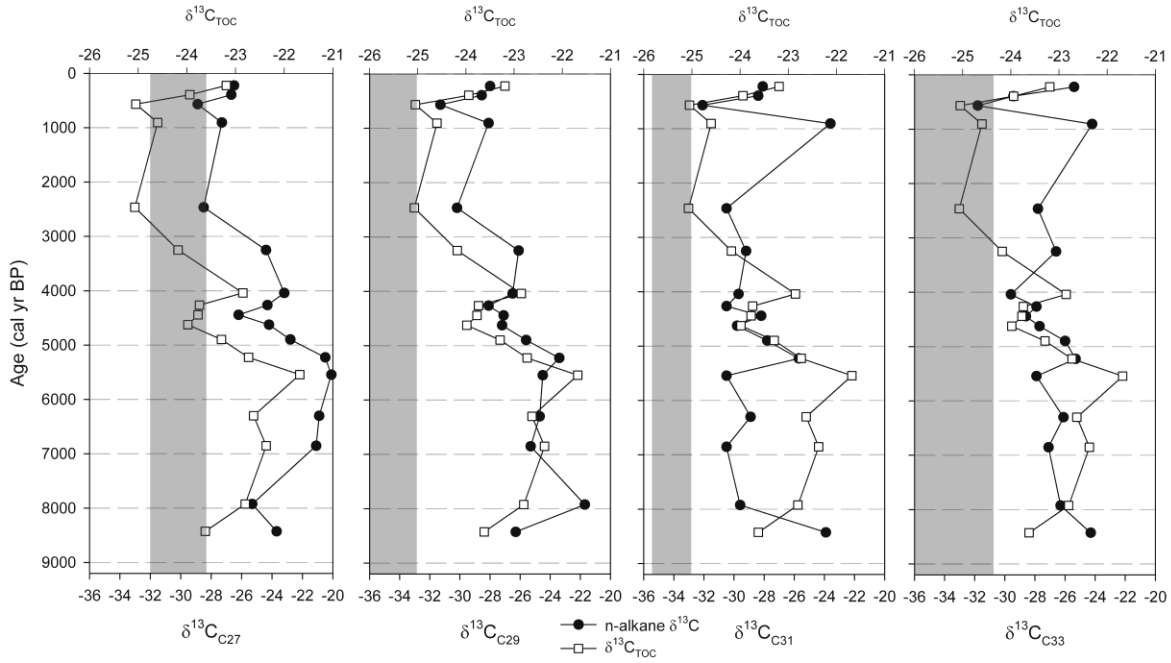

315

316 **Fig. 4** KFN2010 down-core variation in *n*-alkane $\delta^{13}C$ for the C_{27}, C_{29}, C_{31} and C_{33} homologues. Note
317 the different x-axis scales. Shading indicates the standard deviation range from the modern soil data
318 for each homologue. These are the measured values, uncorrected for the Suess effect

319 **Macromolecular organic matter (py-GC/MS)**

320 Pyrolysis-GC/MS analysis produced an array of GC-amenable organic compounds, with between 95
321 and 124 compounds identified in any single sample. These individual compounds were classified
322 into one of seven categories, relating to their basic structure and/or likely precursor compounds
323 (Kaal et al. 2007; Carr et al. 2010, 2013). These comprise aromatic compounds, aliphatics (straight or
324 branched hydrocarbons), lignin products (specific products of lignin monomers), phenols (which may
325 be products of various precursor compounds, including lignin), nitrogen-containing compounds,
326 polyaromatic hydrocarbons, known pyrolysis products of polysaccharides, and sulphur-containing
327 compounds (ESM Table 2**)**.

328 The KFN2010 pyrolysis products are dominated proportionally by aromatic and aliphatic
329 compounds (Fig. 5). The former are low-molecular-weight compounds such as xylene, styrene,

The final publication is available at Springer via http://dx.doi.org/10.1007/s10933-015-9833-7

indene and various methyl benzenes. Because of their lack of functional groups and their potential formation via rearrangements during pyrolysis, they cannot be linked to specific precursor macromolecules. They tend, however, to be the more dominant pyrolysis products in low-TOC samples and the relative abundance of aromatic pyrolysis products is negatively correlated (n=21, r=-0.64, p<0.01) with TOC. Aromatic products are most abundant prior to 8,000 cal yr BP and 4,000-3,000 cal yr BP, and least abundant 6,000-4,500 cal yr BP. The aliphatic class is dominated by *n*-alkane and *n*-alkene doublets that span the range C_7-C_{32} and also includes fatty acids (C_{14}-C_{18}), which show a marked peak in occurrence *ca*. 5,500 cal yr BP. Generally, aliphatics are most abundant 7,500-4,000 cal yr BP, with a secondary peak at 1,800 cal yr BP, although the variation is relatively subtle. These products may have multiple precursors. Longer-chain-length doublets have been associated with specific sources, including plant-derived macromolecules from roots (suberan) and leaves (cutin and cutan), algal lipids, bound leaf wax lipids or post-depositionally formed geopolymers. They can be selectively preserved relative to precursors of other pyrolysis products, which may contribute to their relative abundance in the older parts of the core.

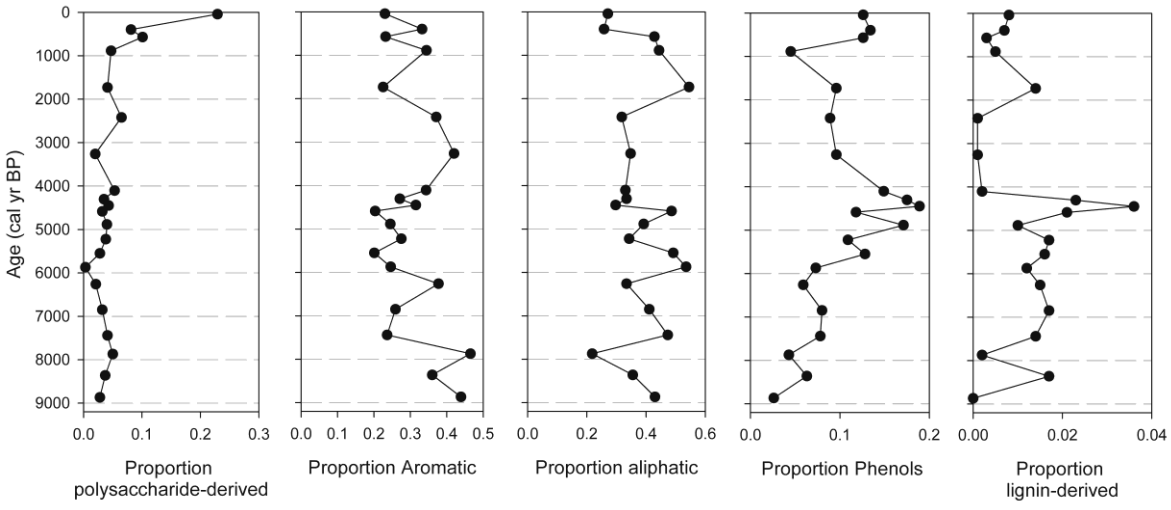

Fig. 5 KFN2010 down-core variation in the major classes of pyrolysis product

Polysaccharide pyrolysis products are consistently found only in the upper 40 cm (the last 1,000 years) of KFN2010 and are most abundant in samples less than 200 years old. They are also

The final publication is available at Springer via http://dx.doi.org/10.1007/s10933-015-9833-7

abundant in the modern Velddrif samples (ESM Table 2; 13-15%). Their down-core reduction is indicative of post-depositional organic matter degradation, consistent with the known susceptibility of polysaccharides to degradation, particularly in semi-arid regions (Nierop et al. 2001; Carr et al. 2013). Similarly, lignin-derived pyrolysis products, which are unequivocal indicators of plant-derived organic matter, but also relatively susceptible to degradation in oxic environments, are generally rare. They are, however relatively more abundant *ca.* 7,400-4,500 cal yr BP, particularly in the interval 5,000-4,000 cal yr BP. Of interest within the KFN2010 pyrolysates is the presence of dimethyl-disulphide and several isomers of dimethylthiophene. These are most abundant 8,000-4,000 cal yr BP. The thiophene ratio (Sinninghe-Damsté et al. 1992) can be used to express their relative abundance (Fig. S5):

$$\textit{Thiophene ratio} = \frac{\text{2,3 dimethylthiophene}}{\text{(1,2-dimethylbenzene + } n\text{-1-nonene)}} \quad (5)$$

Dimethyl-disulphide and dimethylthiophenes are not seen in pyrolysates of terrestrial soil organic matter in the study region (Carr et al. 2013) or in the Velddrif salt marsh sediments (Table S2).

Multivariate analysis of the KFN pollen record

Fifty-one pollen types were identified in the KFN1996 record (Meadows and Baxter 2001). These data were interpreted in terms of the proportions of vlei vegetation, grass pollen (both large and small classes), and to a lesser extent, in terms of shifts in the proportion of dryland Fynbos and scrub forest pollen categories (Meadows and Baxter 2001). The pollen counts (minus exotics and unidentified pollen) were summarised using detrended correspondence analysis (DCA), to isolate the major trends in the pollen record and to generate summary variables for comparison with the geochemical data. The resulting data reveal that the majority of variation within the pollen data (i.e. axis 1; ESM Fig. 6) reflects the relative abundances of Poaceae, Chenopodiaceae and *Limonium* sp. relative to *Typha* sp., Cyperaceae, Santalaceae (*Thesium* is a probable genus), *Myrica* sp. and

The final publication is available at Springer via http://dx.doi.org/10.1007/s10933-015-9833-7

Hermannia sp. (ESM Fig. 6). The DCA axis scores imply a contrast between salt-tolerant plants (Chenopodiaceae and *Limonium* sp., and large-morphology Poaceae pollen) and freshwater riparian/wetland vegetation, notably *Typha* sp. and Cyperaceae. DCA axis 1 sample scores show comparable trends, given the age model uncertainties between the two cores, with $\delta^{13}C_{TOC}$ from KFN2010 (Fig. 6), particularly prior to 3,000 cal yr BP. Axis 2 sample scores show marked changes at *ca*. 3,000 cal yr BP and in the last 1,000 years.

Discussion

Proxy synthesis

By every measure, the sediment record from Klaarfontein reveals distinct changes in organic matter character and stable isotope composition, suggesting profound shifts in conditions during the last *ca*. 8,000 years and a clear distinction between the early and late Holocene at *ca*. 4,300 cal yr BP. TOC/TN ratios and $\delta^{13}C_{TOC}$ have been used in lacustrine, estuarine and salt marsh environments to differentiate marine-derived/algal-derived organic matter (low TOC/TN higher $\delta^{13}C$) from terrestrial plant-derived organic matter (higher TOC/TN, lower $\delta^{13}C$) (Meyers 1997; Lamb et al. 2004). Here, the terrestrial soil SV3 and SV5 TOC/TN ratios (11 ± 2) are relatively low compared to terrestrial plants (Meyers 1997), but they are comparable to soils elsewhere in the Fynbos biome, as are their $\delta^{13}C_{TOC}$ values (Carr et al. 2013). $\delta^{13}C_{TOC}$ from the Velddrif salt marsh is marginally higher than terrestrial soils, averaging -23 ± 1 ‰, whereas TOC/TN is comparable (12 ± 4). The KFN2010 TOC/TN and $^{13}C_{TOC}$ data are suggestive of a dominantly terrestrial or riparian plant organic matter source throughout the Holocene (Meyers 1997), although sediments deposited after 4,000 cal yr BP tend to be associated with higher TOC/TN and lower $\delta^{13}C_{TOC}$ compared to those deposited prior to 4,000 cal yr BP (ESM Fig. 7).

The final publication is available at Springer via http://dx.doi.org/10.1007/s10933-015-9833-7

396 In the pollen data, much of the variability reflects the abundance of halophytic verses
397 freshwater wetland/riparian vegetation, as illustrated by DCA axis 1 (ESM Fig. 6). Meadows and
398 Baxter (2001) argued that in the Verlorenvlei system (Meadows et al. 1994) the large (>50 µm)
399 Poaceae palynomorph is derived from *Spartina maritima* and/or *Sporobolus sp.*, both of which utilise
400 the C_4 photosynthetic pathway. *Spartina alterniflora* has measured leaf tissue $\delta^{13}C$ of -12 to -14 ‰
401 (Wang et al. 2003). This >50-µm subset of Poaceae pollen is also positively correlated with the
402 abundance of Chenopodiaceae pollen, which in this region includes C_4 genera such as *Salsola* sp.
403 (13.6 ‰; Boom et al. 2014). Despite potential differences in the age models (fewer radiocarbon ages
404 for KFN1996), trends in $\delta^{13}C_{TOC}$ from KFN2010 largely mirror DCA axis 1 from KFN1996, suggesting
405 that the abundance of *Spartina*/*Sporobolus*/Chenopodiaceae is indeed a major control on down-core
406 $\delta^{13}C_{TOC}$ variation (Fig. 6). This interpretation further implies that under certain circumstances, i.e.
407 perennial, but potentially saline wetlands, C_4 vegetation may contribute significantly to sediment
408 OM within South Africa's otherwise C_3-dominant winter rainfall region. The relationship between
409 DCA axis 1 and $\delta^{13}C_{TOC}$ is less strong in the last 3,000 years, which may in part reflect some
410 differences in the age models for the two cores, but from 1,500 cal yr BP, DCA axis 2 (increasing
411 significance of several aquatic pollen types verses *Juncus* sp.; ESM Fig. 6) closely tracks $\delta^{13}C_{TOC}$ and
412 the steady reduction in TOC/TN.

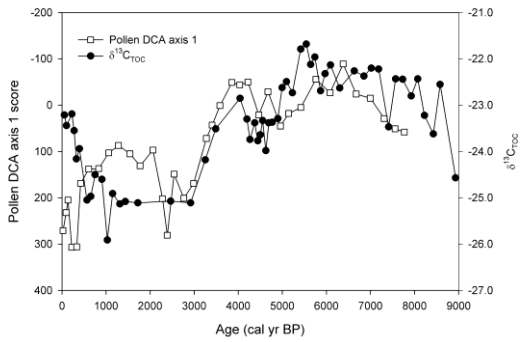

413

414 **Fig. 6** DCA axis 1 sample scores for KFN1996 plotted with $\delta^{13}C_{TOC}$ for KFN2010. The first-order
415 variations in the two records show good correspondence, despite the coarser-resolution age model
416 for KFN1996

The final publication is available at Springer via http://dx.doi.org/10.1007/s10933-015-9833-7

Leaf waxes and *n*-alkane $\delta^{13}C$

The sediment *n*-alkane (leaf wax) distributions indicate substantial contributions from the C_{23}-C_{25} *n*-alkanes and their relative abundance is the main driver of variability in overall *n*-alkane distributions. The variability in the shorter chain length (C_{23}-C_{27}) *n*-alkanes thus suggests changing inputs from emergent/aquatic vegetation and potentially, given some of the similarities with Velddrif, salt-marsh vegetation on or around the site, particularly *ca*. 6,000-3,000 cal yr BP. The abundances of the C_{31}-C_{33} *n*-alkanes are less variable and their ratios remain comparable to contemporary terrestrial vegetation throughout. The $\delta^{13}C$ values for C_{23}-C_{29} *n*-alkanes show strong correlations with each other and with $\delta^{13}C_{TOC,}$ suggesting a common carbon source (Zhang et al. 2004). This implies that wetland and/or riparian vegetation types are probably the primary driver of the bulk isotopic signature and leaf wax distribution (Tanner et al. 2010). Although considerable caution is required when inferring chemotaxonomic effects, the C_{29} *n*-alkane is reported to be strongly dominant in leaf wax distributions for *Spartina alterniflora*, which is closely related to *S. maritima* (Tanner et al. 2010), supporting this interpretation.

In terms of the leaf wax distributions, only the indices relating to the relative abundance of the longest chain length homologues (C_{31} and C_{33}) show any statistically significant correlations with the bulk OM variables; specifically, the relative abundance of C_{31} and C_{33} (defined by Norm31 or $ACL_{27\text{-}33}$) is negatively correlated with $\delta^{13}C_{TOC}$. Thus, more abundant longer chain lengths are associated with lower $\delta^{13}C_{TOC}$ and higher TOC/TN, implying that during times of reduced aquatic/riparian inputs there may be increased contributions from terrestrial plant-derived waxes, which are known to be rich in C_{31} and C_{33} in this region (Carr et al. 2014).

Given the dominance of the C_{31} and C_{33} *n*-alkanes in the regional terrestrial vegetation and the potentially wide dispersal of leaf waxes (Rommerskirchen et al. 2003), the $\delta^{13}C_{C31}$-$\delta^{13}C_{C33}$ signature might therefore be assumed to derive from and reflect a regional vegetation source (Yamamoto et al. 2010; Gao et al. 2011). However, the absolute C_{31} and C_{33} $\delta^{13}C$ values are mostly

The final publication is available at Springer via http://dx.doi.org/10.1007/s10933-015-9833-7

higher than terrestrial vegetation/soil end-member values (i.e. -35 ± 2 ‰ and -34 ± 1 ‰; Table 1) even with a possible ~2‰ Suess effect correction (Garcin et al. 2014). It is therefore likely that the isotope signature from the C_{31} and C_{33} still conflates several sources of leaf wax. Combined with the absence of any correlation between $\delta^{13}C_{C31}$-$\delta^{13}C_{C33}$ and $\delta^{13}C_{TOC}$ and their relatively high $\delta^{13}C$ throughout the record, we that infer the patterns in the C_{31} and C_{33} leaf wax signals probably reflect time-varying contributions from both wetland and terrestrial plant waxes. This would render their proxy environmental signal ambiguous, which may have implications for studies in comparable settings (Wang et al. 2013). This needs to be tested further, particularly through the analysis of *n*-alkane distributions and $\delta^{13}C$ from modern salt-marsh sediments and vegetation, perhaps in conjunction with analysis of δD as a means to assess differences in source waters.

Sea-level change

A noteworthy feature of the py-GC/MS data is the evidence for organically bound sulphur within the sediments. The sulphur itself probably originates from microbial reduction of sulphate in the sediment matrix and incorporation into organic matter during early diagenesis (Sinninghe-Damsté et al. 1992; Hartgers et al. 1997; Lückge et al. 2002). Down-core trends in the thiophene ratio (Fig. ESM 5 and Fig. 7) imply increased incorporation of sulphur 8,500-4,000 cal yr BP and the ratio is significantly correlated with $\delta^{13}C_{TOC}$ ($n= 22$, $r= 0.7$, $p <0.001$). In this context, marine incursions could provide an initial source of sulphur (i.e. sulphate) (Hartgers et al. 1997) and we interpret the thiophene ratio as indicative of relatively greater marine influence within the Verlorenvlei lake and river system 8,500-4,000 cal yr BP. As the incorporation of sulphur into the organic matrix can occur within the sediment column and not just the surface material (Lückge et al. 2002), and can be controlled to some extent by the character (functional group availability) of the host organic matter, the thiophene ratio is interpreted as indicative of general trends in marine influence rather than as a direct measure of relative sea level. High thiophene ratios are coeval with increased abundance of long-chain aliphatics, lignin pyrolysis products and pyrolysis products indicative of contributions from photosynthetic organisms, e.g. Prist-1-ene and Prist-2-ene, which are likely to be derived from

The final publication is available at Springer via http://dx.doi.org/10.1007/s10933-015-9833-7

chlorophyll (Ishiwatari et al. 1991). The increased abundance of lignin pyrolysis products, which are rapidly degraded in semi-arid aerobic conditions (Carr et al. 2010), suggests an environment at the site that may have been at least periodically anoxic and inundated, though not necessarily inundated by sea water. The $\delta^{13}C_{TOC}$ and pollen data are strikingly consistent with the thiophene ratio record (ESM Figs. 5,7), lending weight to this interpretation.

To test this further, the KFN2010 $\delta^{13}C_{TOC}$ and thiophene ratio data were plotted with data pertaining to Holocene sea-level change on the South African and Namibian west coasts (Fig. 7; Miller et al. 1995; Compton 2001, 2006, 2007). Although the thiophene data cannot serve as sea-level index points, they demonstrate generally good correspondence with the geomorphic evidence from which Compton (2001) inferred an early to middle Holocene high stand *ca*. 8,000-5,500 cal yr BP. KFN2010 suggests a distinct reduction in marine influence after 4,300 cal yr BP. This is somewhat later than the Compton (2001) synthesis, but is consistent with radiocarbon ages from back-beach and storm beach deposits at the Verlorenvlei Estuary mouth (Miller et al. 1993, 1995), which constrain the age of the bar at the estuary mouth. This increased marine influence in Verlorenvlei 8,000-4,300 cal yr BP also corresponds with the nearby Elands Bay Cave occupational hiatus (*ca*. 8,700-4,800 cal BP), which has been associated with a reduction in the availability of fresh water (Parkington et al. 1988). Similarly, at nearby Tortoise Cave the later sea-level regression coincides with reduced collection of the estuarine-dwelling *Solan capensis* (razor clam) after *ca*. 4,500 cal BP (Jerardino 1993; Miller et al. 1995). These correspondences suggest some potential for the wider use of the thiophene ratio as an indicator of relative marine influence in comparable depositional environments.

The final publication is available at Springer via http://dx.doi.org/10.1007/s10933-015-9833-7

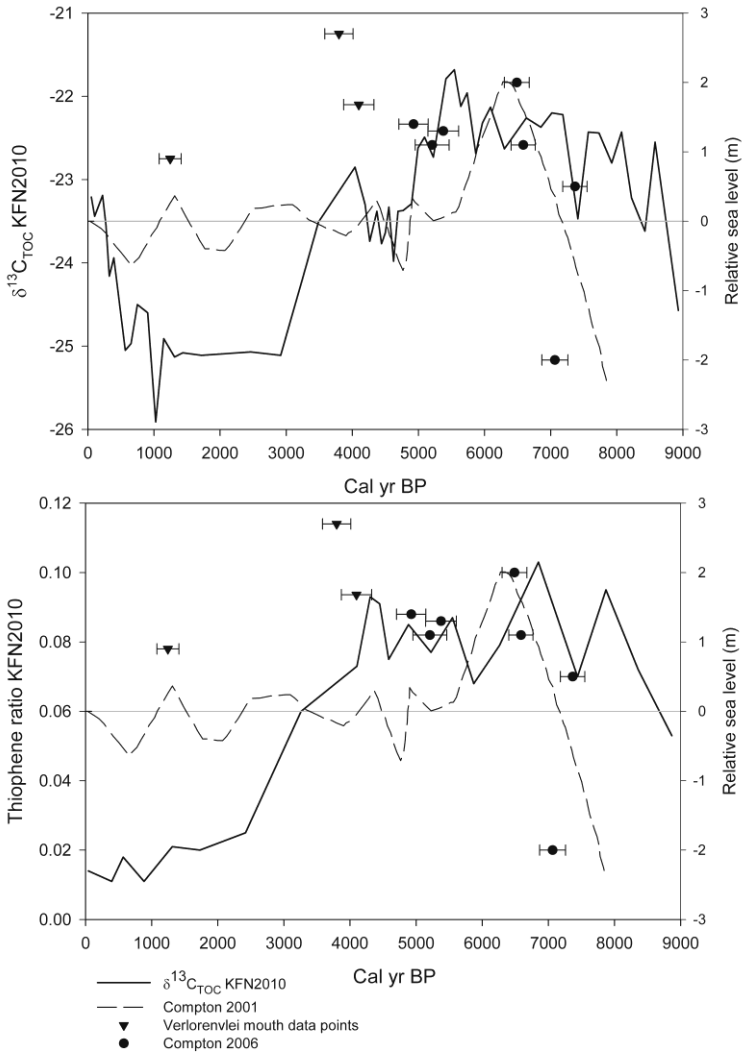

Fig. 7 Trends in marine inundation/influence at KFN2010 as recorded by $\delta^{13}C_{TOC}$ (top) and the thiophene ratio (bottom). Individual data points represent sea-level indicators reported in Miller et al. (1995; inverted triangles; Pta4299 - Verlorenvlei Mouth Sounding and Pta4041 - Public Resort 1 Sounding 1) and Compton (2006) (all data circles). Radiocarbon ages from individual marine shells were re-calibrated using the MARINE13 calibration curve (Reimer et al. 2013) and ΔR estimates for the west coast (Dewer et al. 2012). The dashed line represents Compton's (2001) synthesised Holocene sea-level record. This plot is based on the original radiocarbon age calibrations and interpretations presented by the author

The final publication is available at Springer via http://dx.doi.org/10.1007/s10933-015-9833-7

Environmental changes following reduced marine influence

Following the reduction in marine influence after 4,300 cal yr BP, P_{aq} and TOC/TN remain high until 2,500 and 1,000 cal yr BP, respectively, implying that wetland/riparian vegetation continued to grow around the site. Correspondingly, the KFN1996 pollen record after 4,000 cal yr BP shows an increased prominence of *Typha sp., Pteridium*-type, Cyperaceae and Aponogetonaceae pollen, particularly *ca*. 3,000 cal yr BP (ESM Figs. 6,8). This shift is apparent in the sample scores of KFN1996 DCA axis 2, with several samples from this period plotting in the lower centre of the diagram (ESM Fig. 8). This has been interpreted as a period of higher moisture availability and reduced salinity (Meadows and Baxter 2001). Despite potential differences in age models, the KFN2010 samples from this period also show lower $\delta^{13}C_{TOC}$ and higher TOC, which might suggest wetter conditions, although perhaps still with some seasonal drying, as indicated by the relatively low significance of more labile pyrolysis products such as lignin (Fig. 5).

The period *ca*. 2,500 - 950 cal yr BP reveals a clear shift in the pollen spectra, with an increase in the abundance of *Juncus* sp. and some succulent pollen types (Meadows and Baxter 2001; ESM Fig. 8), as well as substantial changes in leaf wax *n*-alkane distributions, notably the P_{aq} index, which declines between 2,000 and 900 cal yr BP, in conjunction with leaf wax $\delta^{13}C$ and $\delta^{13}C_{TOC}$. TOC content also drops to a minimum (Fig. 2). Overall, the period *ca*. 2,500-950 cal yr BP was drier than 4,000-2,500 cal yr BP and was characterised by more terrestrial-like plant leaf wax distributions (Fig. 3 and ESM Fig. 4). The pollen assemblages are more characteristic of karroid-type vegetation (ESM Fig. 6), as are the Norm31 and CPI data, which at 900 cal yr BP are consistent with an increased occurrence of karroid vegetation (Carr et al. 2014).

Comparisons of the middle to late Holocene data from KFN2010, i.e. post marine influence, with other palaeoenvironmental records, indicate some regional similarities, although the uncertainties in the KFN2010 age model 4,000-2,000 cal yr BP should be kept in mind. The charcoal record from the adjacent Elands Bay Cave indicates low percentages of xeric thicket types at ~3,500

524 cal yr BP, followed by their increased significance across the late Holocene, particularly after 1,300
525 cal yr BP (Cowling et al. 1999). Similar conclusions have been drawn from the pollen and micro-
526 charcoal records from the De Rif rock hyrax middens, 64 km to the west in the Cederberg Mountains
527 (Valsecchi et al. 2013) and from Princess Vlei, 13 km SSW of Cape Town on the Cape Flats (Neumann
528 et al. 2011), both of which indicate a trend toward drier conditions and increased seasonality after
529 ~3,000 cal yr BP. This shift to drier late Holocene conditions may be related to lower coastal sea-
530 surface temperatures in the Benguela system after 3,500 cal yr BP (Farmer et al. 2005), which are
531 likely linked to increased upwelling and increased summer drought season length/intensity.
532 Considering the site's position in the winter rainfall zone, and data indicating an elevated influence
533 of the Southern Hemisphere westerlies at that time (Chase et al. 2013; Lamy et al. 2001), such
534 interpretations seem inconsistent. However, changes in coastal SSTs and upwelling have been shown
535 to be significant for regional hydro-climates (Chase et al. 2011), and it may be that coastal sites and
536 associated flora such as at Klaarfontein, Verlorenvlei, Elands Bay Cave and Princess Vlei, are sensitive
537 to the enhanced summer drought that increased upwelling may engender. This is supported by
538 contrasting trends seen in the transitional summer-winter rainfall zone 120 km southeast of
539 Verlorenvlei, where we see a weak trend from relatively drier conditions 3,500-2,500 cal yr BP to
540 more humid conditions 2,500 cal BP (Chase et al. 2015). Such changes were interpreted to have
541 been driven by the varying impact of easterly-derived rainfall and the distinct contrast with the late
542 Holocene trends in KFN2010 implies a minimal role for easterly anomalies on the west coast.

543 The last 500 years see a marked shift in the KFN2010 record, with higher $\delta^{13}C$, lower TOC/TN
544 ratios, higher P_{aq} and higher TOC and decreasing DCA axis 2 scores (more aquatic, less *Juncus* sp. and
545 succulent pollen types; ESM Figs. 6,8). This corresponds with previous observations at Grootdrift
546 (Meadows et al. 1996). *Myriophyllum spicatum* (Aponogetonaceae) is historically abundant in this
547 part of the Verlorenvlei system (Sinclair et al. 1986) and its increased abundance may explain the
548 lower DCA axis 2 sample scores. A high-resolution diatom record from Verlorenvlei (Stager et al.
549 2012) also provides a more detailed picture of environmental change during the last 1,000 years,

The final publication is available at Springer via http://dx.doi.org/10.1007/s10933-015-9833-7

with an increased presence of brackish and epiphytic diatoms during a relatively dry Medieval Warm Period, consistent with the aforementioned period of aridity identified in the leaf wax data, followed by an increase in lower-salinity diatoms after ~950 cal yr BP. This period of increasingly wetter conditions, which is associated with an increasing P_{aq} in KFN2010, culminated during the Little Ice Age at AD 1850, whereupon brackish conditions returned (Stager et al. 2012).

Conclusions

Klaarfontein presently provides one of the few long Holocene sediment archives on the west coast lowlands of South Africa. In this study, combined stable isotope and biogeochemical analyses, integrated with the existing pollen data, provide insights into the relations between multiple organic matter fractions, pollen data and depositional environments. The data are particularly indicative of a vegetation response to varying salinity around Klaarfontein, which was strongly affected by marine inundation. We propose that the timing and relative influence of marine incursions can be further constrained by the thiophene ratio, which provides indirect evidence for marine inundation via evidence for the incorporation of reduced sulphur into macromolecular organic matter. The results are broadly consistent with independent evidence for relative sea-level change on the South African west coast, suggesting that this approach may be more widely applicable, although further validation with other trace element data is needed. The suggestion that a subset of the pollen data (the large Poaceae palynomorphs) is representative of C_4 grasses *Spartina maritima* and/or *Sporobolus* sp., is now supported by the stable isotope data. This demonstrates that localised C_4 vegetation can contribute to sediment organic matter within the otherwise C_3 ecosystems of the winter rainfall zone. Furthermore, the over-riding contribution of locally derived organic matter means that the interpretative problems associated with the dominance of locally derived pollen types are somewhat mirrored in the analysis of leaf wax lipids. The stable carbon isotope data from leaf wax *n*-alkanes require careful interpretation given the variable contributions from local riparian and wider terrestrial plant leaf wax sources.

The final publication is available at Springer via http://dx.doi.org/10.1007/s10933-015-9833-7

Overall, there is a clear distinction in the KFN2010 record between the early-middle Holocene and the late Holocene. During the late Holocene (4,000 cal yr BP to present), when the marine influence on Verlorenvlei was much reduced, the geochemical and chronological data support previous interpretations from palynological data in suggesting a period of increased water availability *ca*. 4,000-2,500 cal yr BP, though some drying of the site is inferred from the py-GC/MS data. This was followed by increasingly arid conditions 2,500-900 cal yr BP. More regular freshwater inundation is apparent within the last 700 years. Supporting evidence for these late Holocene trends is seen in the wider palaeoenvironmental record and these new data contribute to an increasingly coherent view of the Holocene environmental history of the Verlorenvlei system.

Acknowledgements

This research was funded by the Leverhulme Trust (Grant F/00 212/AF). B.M.C. received additional support from the European Research Council (ERC), under the European Union's Seventh Framework Programme (FP7/2007e2013)/ERC Starting Grant "HYRAX" (Grant agreement no. 258657). We thank Professor Judith Sealy for helpful discussion and for providing some literature. Two anonymous reviewers are also thanked for very useful comments.

References

Aichner B, Herzschuh U, Wilkes H (2010) Influence of aquatic macrophytes on the stable carbon isotopic signatures of sedimentary organic matter in lakes on the Tibetan Plateau. Org Geochem 41: 706–718

Baxter AJ (1997) Late Quaternary palaeoenvironments of the Sandveld, Western Cape Province, South Africa. Unpublished PhD thesis, University of Cape Town

Baxter AJ, Meadows ME (1994) Palynological evidence for the impact of colonial settlement within lowland fynbos: a high resolution study from the Verlorenvlei, southwestern Cape Province, South Africa. Hist Biol 9: 61-70

The final publication is available at Springer via http://dx.doi.org/10.1007/s10933-015-9833-7

599 Baxter AJ, Meadows ME (1999) Evidence for Holocene sea-level change at Verlorenvlei, Western
600 Cape, South Africa. Quat Int 56: 65-79

601 Blaauw M, Christen JA (2011) Flexible Paleoclimate Age-Depth Models Using an Autoregressive
602 Gamma Process. Bayesian Analysis 6: 457-474

603 Boom A, Carr AS, Chase BM, Grimes HL, Meadows ME (2014) Leaf wax *n*-alkanes and $\delta^{13}C$ values of
604 CAM plants from arid southwest Africa. Org Geochem 67: 99-102

605 Bray EE, Evans ED (1961) Distribution of *n*-paraffins as a clue to recognition of source beds. Geochim
606 Cosmochim Ac 22: 2–15

607 Carr AS, Boom A, Chase BM, Roberts DL, Roberts ZE (2010) Molecular fingerprinting of wetland
608 organic matter using pyrolysis-GC/MS: an example from the southern Cape coastline of
609 South Africa. J Paleolimnol 44: 947-961

610 Carr AS, Boom A, Chase BM, Meadows ME, Roberts ZE, Britton MN, Cumming AMJ (2013) Biome-
611 scale characterisation and differentiation of semi-arid and arid zone soil organic matter
612 compositions using pyrolysis-GC/MS analysis. Geoderma 200-201: 189-201

613 Carr AS, Boom A, Grimes HL, Chase BM, Meadows ME, Harris A (2014) Leaf wax *n*-alkane
614 distributions in arid zone South African flora: Environmental controls, chemotaxonomy and
615 palaeoecological implications. Org Geochem 67: 72-84

616 Chase BM, Meadows ME (2007) Late Quaternary dynamics of southern Africa's winter rainfall zone.
617 Earth Sci Rev 84: 103-138

618 Chase BM, Quick LJ, Meadows ME, Scott L, Thomas DSG, Reimer PJ (2011) Late glacial inter-
619 hemispheric climate dynamics revealed in South African hyrax middens. Geology 39: 19-22

620 Chase BM, Boom A, Carr AS, Meadows ME, Reimer PJ (2013) Holocene climate change in
621 southernmost South Africa: rock hyrax middens record shifts in the southern westerlies.
622 Quat Sci Rev 82: 199–205

623 Chase BM, Lim S, Chevalier M, Boom A, Carr AS, Meadows ME, Reimer PJ (2015) Influence of tropical
624 easterlies in southern Africa's winter rainfall zone during the Holocene. Quat Sci Rev 107:
625 138-148

626 Compton JS (2001) Holocene sea-level fluctuations inferred from the evolution of depositional
627 environments of the southern Langebaan Lagoon salt marsh, South Africa. Holocene 11:
628 395–405

629 Compton JS (2006) The mid-Holocene sea-level high stand at Bogenfels Pan on the southwest coast
630 of Namib. Quat Res 66: 303-310

631 Compton JS (2007) Holocene evolution of the Anichab Pan on the southwest coast of Namibia.
632 Sedimentology 54: 55-70

633 Cowling RM, Cartwright CR, Parkington JE, Allsopp, JC (1999) Fossil wood charcoal assemblages from
634 Elands Bay Cave, South Africa: implications for late Quaternary vegetation and climates in
635 the winter-rainfall Fynbos biome. J Biogeog 26: 367-378

636 de Leeuw JW, Versteegh GJM, van Bergen PF (2006) Biomacromolecules of algae and plants and
637 their fossil analogues. Plant Ecol: 182, 209-233

638 Dewer G, Reimer PJ, Sealy J, Woodborne S (2013) Late-Holocene marine radiocarbon reservoir
639 correction (ΔR) for the west coast of South Africa. Holocene 22: 1481-1489

640 Farmer EC, deMenocal PB, Marchitto TM (2005) Holocene and deglacial ocean temperature
641 variability in the Benguela upwelling region: Implications for low-latitude atmospheric
642 circulation. Paleoceanography 20: doi: 10.1029/2004PA001049

643 Ficken KJ, Li B, Swain DL, Eglinton G (2000) An *n*-alkane proxy for the sedimentary input of
644 submerged/floating freshwater aquatic macrophytes. Org Geochem: 31, 745-749

645 Gao L, Hou, J, Toney J, MacDonald D, Huang Y (2011) Mathematical modeling of the aquatic
646 macrophyte inputs of mid-chain n-alkyl lipids to lake sediments: Implications for interpreting
647 compound specific hydrogen isotopic records. Geochim Cosmochim Ac 75: 3781-3791

648 Garcin Y, Schefuß E, Schwab, VF, Garreta V, Gleixner G, Vincens A, Todou G, Séne´ O, Onana J-M,
649 Achoundong G, Sachse D (2014) Reconstructing C_3 and C_4 vegetation cover using n-alkane
650 carbon isotope ratios in recent lake sediments from Cameroon, Western Central Africa.
651 Geochim Cosmochim Ac 142: 482-500

652 Hammer Ø, Harper DAT, Ryan PD (2001) PAST: Paleontological statistics software package for
653 education and data analysis. Palaeontol Electron 4: 9 pp

654 Hartgers WA, Lopez JF, Sinninghe-Damste´ JS, Reiss C, Maxwell JR, Grimalt JO (1997) Sulfur-binding
655 in recent environments: II. Speciation of sulfur and iron and implications for the occurrence
656 of organo-sulfur compounds. Geochim Cosmochim Ac 61: 4769–4788

657 Hogg AG, Hua Q, Blackwell PG, Niu M, Buck CE, Guilderson TP, Heaton TJ, Palmer JG, Reimer PJ,
658 Reimer RW, Turney CSM, Zimmerman SRH (2013) SHCal13 Southern Hemisphere Calibration,
659 0–50,000 Years cal BP. Radiocarbon 55: 1889-1903

660 Horowitz A (1992) Palynology of Arid Lands. Elsevier, Amsterdam

661 Ishiwatari M, Ishiwatari R, Sakashita H, Tatsumi T, Tominaga H (1991) Pyrolysis of chlorophyll-a after
662 preliminary heating at a moderate temperature: implications for the origins of Prist-1-ene on
663 kerogen pyrolysis. J Anal Appl Pyrolysis 18: 207-218

664 Jerardino A (1993) Mid- to late Holocene sea-level fluctuations: the archaeological evidence at
665 Tortoise Cave, south-western Cape, South Africa. S Afr J Sci 89: 481–488

666 Kaal J, Baldock JA, Buurman P, Nierop KGJ, Pontevedra-Pombol X, Martínez-Cortizas AM (2007)
667 Evaluating pyrolysis-GC/MS and ^{13}C CPMAS NMR in conjunction with a molecular mixing
668 model of the Penido Vello peat deposit, NW Spain. Org Geochem 38: 1097-1111

669 Kaal, J, Schellekens, J, Nierop, KGJ, Martínez Cortizas A, Muller J (2014) Contribution of organic
670 matter molecular proxies to interpretation of the last 55 ka of the Lynch's Crater record (NE
671 Australia) Palaeogeogr Palaeoclimatol Palaeoecol 414: 20-31

672 Lamb AL, Leng MJ, Mohammed MU, Lamb HF (2004) Holocene climate and vegetation change in the
673 Main Ethiopian Rift Valley, inferred from the composition (C/N and $\delta^{13}C$) of lacustrine
674 organic matter. Quat Sci Rev 23: 881-891

675 Lamy F, Hebbeln D, Rohl U, Wefer G (2001) Holocene rainfall variability in southern Chile: a marine
676 record of latitudinal shifts of the Southern Westerlies. Earth Planet Sci Lett 185: 369-382

677 Lückge A, Horsfield B, Littke R, Scheeder G (2002) Organic matter preservation and sulfur uptake in
678 sediments from the continental margin off Pakistan. Org Geochem 33: 477-488

679 Meadows ME, Baxter AJ, Adams T (1994) The Late Holocene vegetation history of the lowland
680 Fynbos, Verlorenvlei, southwestern Cape, South Africa. Hist Biol 9: 47-58

The final publication is available at Springer via http://dx.doi.org/10.1007/s10933-015-9833-7

681 Meadows ME, Osmal A (1996) Chronology, sedimentology and geochemistry of sediments at
682 Verlorenvlei (Western Cape Province, South Africa) as evidence of anthropogenically-
683 induced land degradation. Z Geomorph Supp Bd 107: 45-62

684 Meadows ME, Baxter AJ, Parkington JE, Adams T (1996) Late Holocene environments at Verlorenvlei,
685 Western Cape Province, South Africa. Quat Int 33: 81-95

686 Meadows ME, Baxter AJ (1999) Evidence for Holocene sea-level change at Verlorenvlei, Western
687 Cape, South Africa. Quat Int 56: 65-79

688 Meadows ME, Baxter AJ (2001) Holocene vegetation history and palaeoenvironments at Klaarfontein
689 Sprints, Western Cape, South Africa. Holocene 11: 699-706

690 Meyers PA (1997) Organic geochemical proxies of paleoceanographic, paleolimnologic, and
691 paleoclimatic processes. Org Geochem 27: 213-250

692 Miller DE, Yates RJ, Parkington JE, Vogel JC (1993) Radiocarbon dated evidence relating a mid
693 Holocene relative high sea-level on the south-western Cape coast, South Africa. S Afr J Sci
694 89: 35-44

695 Miller DE, Yates RJ, Jerardino A, Parkington JE (1995) Late Holocene coastal change in the
696 southwestern Cape, South Africa. Quat Int 29/30: 3-10

697 Nierop KGJ, Pullema, MM, Marinissen JCY (2001) Management induced organic matter
698 differentiation in grassland and arable soil: a study using pyrolysis techniques. Soil Biol
699 Biochem 33: 755-764

700 Neumann FH, Scott L, Bamford MK (2011) Climate change and human disturbance of fynbos
701 vegetation during the late Holocene at Princess Vlei, Western Cape, South Africa. Holocene
702 21: 1137-1149

703 Parkington JE, Poggenpoel C, Buchanan W, Robey T, Manhire A, Sealy J (1988) Holocene coastal
704 settlement patterns in the Western Cape. In: Bailey G, Parkington, JE (Eds). The Archaeology
705 of Prehistoric Coastlines. Cambridge University Press, 22-41

706 Parkington JE (2012) Mussels and mongongo nuts: logistical visits to the Cape west coast, South
707 Africa. J Archaeol Sci 39: 1521-1530

708 Poynter JG, Farrimond P, Brassell SC, Eglinton G (1989) Aeolian-derived higher plant lipids in the
709 marine sedimentary record: Links with paleoclimate. In: Leinen M, Sarnthein M (Eds),
710 Palaeoclimatology and Palaeometeorology: Modern and Past Patterns of Global Atmosphere
711 Transport. NATO ASI Series D, Kluwer, pp 435–462

712 Reimer PJ, Bard E, Bayliss A, Beck JW, Blackwell PG, Ramsey CB, Buck CE, Cheng H, Edwards RL,
713 Friedrich M, Grootes PM, Guilderson TP, Haflidason H, Hajdas I, Hatté C, Heaton TJ,
714 Hoffmann DL, Hogg AG, Hughen KA, Kaiser KF, Kromer B, Manning SW, Niu M, Reimer RW,
715 Richards DA, Scott EM, Southon JR, Staff RA, Turney CSM, Plicht JvD, (2013) IntCal13 and
716 Marine13 radiocarbon age calibration curves 0-50,000 years cal BP. Radiocarbon 55: 1869–
717 87

718 Rommerskirchen F, Eglinton G, Dupont L, Güntner U, Wenzel C, Rullkötter J (2003) A north to south
719 transect of Holocene southeast Atlantic continental margin sediments: relationship between
720 aerosol transport and compound specific $\delta^{13}C$ land plant biomarker and pollen records.
721 Geochem Geophy Geosy 4: 1101

722 Saiz-Jimenez C, de Leeuw JW (1987) Chemical characterization of soil organic matter fractions by
723 analytical pyrolysis–gas chromatography–mass spectrometry. J Anal Appl Pyrolysis 9: 99–119

The final publication is available at Springer via http://dx.doi.org/10.1007/s10933-015-9833-7

724 Scott L, Woodborne S (2007) Vegetation history inferred from pollen in late Quaternary faecal
725 deposits (hyraceum) in the Cape winter-rain region and its bearing on past climates in South
726 Africa. Quat Sci Rev 26: 941-953

727 Sinclair SA, Lane SB, Grindley JR (1986) Verlorenvlei. Report 32 in Estuaries of the Cape, edited by:
728 Heydorn AEF, Morant, PD, CSIR Research Report 431 96p

729 Sinninghe-Damsté JS, de las Heras FXX, de Leeuw JW (1992) Molecular analysis of sulphur-rich
730 brown coals by flash pyrolysis-gas chromatography-mass spectrometry. J Chromatogr
731 607: 361-376

732 Stager JC, Mayewski PA, White J, Chase BM, Neumann FH, Meadows ME, King CD, Dixon DA (2012)
733 Precipitation variability in the winter rainfall zone of South Africa during the last 1400 yr
734 linked to the austral westerlies. Clim Past 8: 877–887

735 Stuiver M, Reimer PJ (1993) Extended ^{14}C data base and revised CALIB 3.0 ^{14}C age calibration
736 program. Radiocarbon 35: 215-230 (version 7.0)

737 Tanner BR, Uhle ME, Mora CI, Kelley JT, Schuneman JJ, Lane CS, Allen, E.A (2010) Comparison of bulk
738 and compound-specific $\delta^{13}C$ analyses and determination of carbon sources to salt marsh
739 sediments using *n*-alkane distributions (Maine, USA). Estuar Coast Shelf Sci 86: 283–291

740 Valsecchi V, Chase BM, Slingsby J, Carr AS, Quick LJ, Meadows ME, Cheddadi R, Reimer PJ (2013) A
741 high resolution 15,600-year pollen and microcharcoal record from the Cederberg Mountains,
742 South Africa. Palaeogeogr Palaeoclimatol Palaeoecol 387: 6-16

743 Vancampenhout K, Wouters K, Caus A, Buurman P, Swennen R, Deckers J (2008) Fingerprinting of
744 soil organic matter as a proxy for assessing climate and vegetation changes in last
745 interglacial palaeosols (Veldwezelt, Belgium). Quat Res. 69: 145–162

746 Wang XC, Chen RF, Berry A (2003) Sources and preservation of organic matter in Plum Island salt
747 marsh sediments (MA, USA): long-chain *n*-alkanes and stable carbon isotope compositions.
748 Estuar Coast Shelf Sci 58: 917-928

749 Wang YV, Larsen T, Leduc G, Andersen N, Blanz T, Schneider R (2013) What does leaf wax δD from a
750 mixed C_3/C_4 vegetation region tell us? Geochim Cosmochim Ac 111: 128–139

751 Yamamoto S, Kawamura K, Seki O, Meyers PA, Zheng Y, Zhou W (2010) Environmental influences
752 over the last 16 ka on compound-specific $\delta^{13}C$ variations of leaf wax *n*-alkanes in the Hani
753 peat deposit from northeast China. Chem Geol 277: 261-268

754 Zhang Z, Zhao N, Yang X, Wang S, Jiang J, Oldfield F, Eglinton G (2004) A hydrocarbon biomarker
755 record for the last 40 kyr of plant input to Lake Heqing, southwestern China. Org Geochem
756 35: 595-613

757

The final publication is available at Springer via http://dx.doi.org/10.1007/s10933-015-9833-7

758 **Table 1:** Results of the *n*-alkane $\delta^{13}C$ analyses for the KFN2010 core and from modern Sandveld soils adjacent to Verlorenvlei. Sites SV3 and SV5 as described in Carr et al. (2014)

Depth (m)	Age (cal yr BP)	$\delta^{13}C_{TOC}$ (‰)	$\delta^{13}C_{c23}$ (‰)	Std. dev (‰)	$\delta^{13}C_{c25}$ (‰)	Std. dev (‰)	$\delta^{13}C_{c27}$ (‰)	Std. dev (‰)	$\delta^{13}C_{c29}$ (‰)	Std. dev (‰)	$\delta^{13}C_{c31}$ (‰)	Std. dev (‰)	$\delta^{13}C_{c33}$ (‰)	Std. dev (‰)
0.2	223	-23.2	-26.8		-25.5	0.2	-26.5	0.3	-28.0	0.6	-28.1	0.4	-25.4	0.7
0.3	393	-23.9					-26.7		-28.6		-28.4		-29.4	
0.4	566	-25.1	-27.7	0.5	-27.7	0.2	-28.9	0.4	-31.3	0.1	-32.1	0.2	-31.8	0.2
0.5	905	-24.6			-25.9		-27.3	0.4	-28.1	0.1	-23.6	0.3	-24.2	0.1
0.8	2464	-25.1	-28.3	0.3	-27.2	1.0	-28.5	0.3	-30.2	0.4	-30.5	0.4	-27.8	0.4
0.9	3251	-24.2	-22.3		-25.2	0.3	-24.4	0.1	-26.1	0.4	-29.2	0.3	-26.6	0.2
1.0	4041	-22.9	-26.0	0.2	-26.2	0.2	-23.2	0.1	-26.5	0.1	-29.7	0.3	-29.6	0.3
1.1	4264	-23.7			-25.0	0.2	-24.3	0.4	-28.1	0.1	-30.5	0.1	-27.9	0.3
1.2	4442	-23.8	-24.2	0.2	-25.8	0.2	-26.2	0.9	-27.1	0.5	-28.2	0.8	-28.6	0.3
1.3	4624	-24.0	-21.5	0.2	-23.3	0.1	-24.2	0.1	-27.2	0.1	-29.8	0.2	-27.7	0.3
1.4	4896	-23.3	-23.9	0.3	-24.3	0.1	-22.8	0.4	-25.6	0.6	-27.8	0.3	-26.0	0.1
1.5	5226	-22.7			-23.5		-20.5	0.4	-23.4	0.3	-25.7	0.6	-25.3	0.5
1.6	5544	-21.7	-20.2	0.2	-22.4	0.1	-20.1	0.1	-24.5	0.1	-30.5	0.1	-27.9	0.3
1.8	6300	-22.6	-19.6	0.2	-21.5	0.3	-20.9	0.2	-24.7	0.1	-28.9	0.3	-26.1	0.2
1.9	6851	-22.4	-19.6	0.4	-22.7	0.1	-21.1	0.1	-25.3	0.1	-30.5	0.1	-27.1	0.4
2.1	7924	-22.8			-26.6	0.3	-25.3		-21.7	0.3	-29.6	0.1	-26.3	0.3
2.2	8425	-23.6					-23.7	0.5	-26.3	0.3	-23.9	0.2	-24.3	0.7
Average			**-23.6 ± 3.2**		**-24.9 ± 1.8**		**-24.4 ± 2.7**		**-26.6 ± 2.4**		**-28.6 ± 2.3**		**-27.2 ± 2.0**	
SV5s1	-	-26.3	-29.4	nd	-29.9	nd	-29.4	nd	-32.3	nd	-32.8	nd	-31.0	nd
SV5s3	-	-25.4	-29.2	0.0	-32.4	0.1	-31.2	0.0	-33.1	0.1	-34.5	0.0	-34.3	0.1
SV5s4	-	-27.2	-26.3	0.4	-30.4	0.3	-31.9	0.2	-36.2	0.5	-36.5	0.2	-37.1	0.1
SV3s4	-	-25.8	-27.3	0.4	-27.3	0.7	-29.5	0.2	-36.0	0.0	-33.4	0.2	-30.9	0.5
SV3s2	-	-25.3	-29.6	nd	-30.3	nd	-28.1	nd	-35.0	nd	-33.8	nd	-34.1	nd
Average		**-26 ± 0.8**	**-28.4 ± 1.5**		**-30.1 ± 1.8**		**-30.0 ± 1.5**		**-34.5 ± 1.7**		**-34.2 ± 1.4**		**-33.5 ± 2.6**	

The final publication is available at Springer via http://dx.doi.org/10.1007/s10933-015-9833-7

759